HYDRODYNAMIC THEORY OF SWIMMING OF FLAGELLATED MICROORGANISMS

JOSE GARCIA DE LA TORRE AND VICTOR A. BLOOMFIELD, *Department of Biochemistry, University of Minnesota, St. Paul, Minnesota 55108 U.S.A.*

ABSTRACT A theory of the type commonly used in polymer hydrodynamics is developed to calculate swimming properties of flagellated microorganisms. The overall shape of the particle is modeled as an array of spherical beads which act, at the same time, as frictional elements. The fluid velocity field is obtained as a function of the forces acting at each bead through Oseen-type, hydrodynamic interaction tensors. From the force and torque equilibrium conditions, such quantities as swimming velocity, angular velocity, and efficiency can be calculated. Application is made to a spherical body propelled by a helical flagellum. A recent theory by Lighthill, and earlier formulations based on tangential and normal frictional coefficients of a curved cylinder, C_T and C_N, are analyzed along with our theory. Although all the theories predict similar qualitative characteristics, such as optimal efficiency and the effect of fluid viscosity, they lead to rather different numerical values. In agreement with Lighthill, we found the formalisms based on C_N and C_T coefficients to be somewhat inaccurate, and head-flagellum interactions are shown to play an important role.

INTRODUCTION

Much of our current understanding of the swimming motion of flagellated microorganisms rests on the pioneering theoretical analysis of Hancock and Gray (1,2). For the helical mode of propulsion, which concerns us in this paper, several applications of the Gray-Hancock theory have been made. Holwill and Burge (3) made a complete calculation of swimming velocities, later modified by Chwang and Wu (4) to take into account rotation of the head and of the cross-section of the flagellum. Using these improvements, Chwang et al. (5) analyzed the peculiar motion of *Spirillum*. Similar work was carried out at the same time by Schneider (6). Recently, Keller and Rubinow (7) have shown that the trajectory of the microorganism is a helix of small radius instead of a straight line. Similar advances have been made in the study of planar, sinusoidal motion. More complete surveys of the field may be found in recent reviews (8–10).

The basis of the Gray-Hancock theory is the hydrodynamic behavior of a long, thin, slightly deformed cylinder under low Reynolds number conditions. A distribution of singular solutions—stokeslets, doublets, rotlets—of the Stokes equation for an inertialess fluid is placed along the center line of the cylinder (1,9) to get the normal and tangential frictional coefficients per unit of length, C_N and C_T. Hancock (1) obtained $C_N/C_T = 2$ for oscillations of small amplitude, the absolute values of C_T and C_N de-

pending on the dimensions of the flagellum. Several attempts have been made to improve the hydrodynamic foundations of Hancock's coefficients and to calculate them for more general cases (9–13).

Very recently, Lighthill (10) has proposed a theory for flagellar propulsion that seems better founded than the previous approaches. Although Lighthill's major results are presented in the form of analytical equations without frictional coefficients, he presents, as a secondary result of his theory, improved values for C_T and C_N that can be used in equations based on the Gray-Hancock formalism (3,4).

An alternative framework for the study of hydrodynamics of particles immersed in incompressible viscous fluids is that introduced by Oseen (14). The fundamental quantity of this theory is the hydrodynamic interaction tensor, which gives the velocity field in the fluid produced by a point force. The Oseen formalism, developed by Kirkwood and Riseman (15,16) has been used for many years to study hydrodynamic properties of macromolecules in solution (17). The image of a linear macromolecule, which resembles a long cylinder of small radius, more or less curved in space, does not differ much from that of a flagellum. We were thus led to wonder to what extent the concepts of macromolecular hydrodynamics apply to flagellar propulsion.

To represent the finite thickness of a macromolecule or flagellum, two kinds of models can be used. In cylindrical models, a continuous distribution of point sources of friction is assumed along the surface of the cylinder. In bead or subunit models the particle is constructed of an array of many spherical elements, whose hydrodynamic behavior is determined by their Stokes' law frictional coefficients and the hydrodynamic interaction tensors between them. We have recently applied bead models to calculate hydrodynamic properties of helical polymers (18) and of bacteriophages with heads, tails, and tail fibers (19–21); the theoretical predictions and experimental data generally agreed. Therefore, we anticipate that bead models should be suitable to study the movement of a particle having a large head and a helical tail. The only difference is that the translation of the particle is caused by an internal motion of the helical propeller, rather than external sedimentation or Brownian motion forces.

In our theory, the Stokes forces associated with the rotatory motion of the beads in the flagellum generate, through hydrodynamic interaction, a velocity perturbation in the fluid that is responsible for the propulsive effect. However, the velocity components of the head and different places on the flagellum are coupled, so that the propulsive contribution varies along the flagellum. These end and neighboring effects were noted by Chwang and Wu (4), but were ignored in their calculations and in most others. We show in this paper how an Oseen-tensor treatment of bead models for flagellated microorganisms allows for a detailed calculation of the velocity field. This makes possible a quantitative evaluation of end and neighboring effects. We also have evaluated in detail the expressions obtained by Lighthill (10), to compare them with our results and with previous calculations (3,4).

This paper, like many others in the field (3–6,9,10) lacks a detailed numerical comparison of theoretical results with experimental data. This is mainly because there is no microorganism of simple shape for which a complete study of geometric and kinematic

parameters has been done. The major purpose of our work is to compare different tbeoretical approaches.

THEORY

Geometry and Motion of the Bead Model for a Helical Flagellum

In the bead model, the helical flagellum is replaced by a discrete array of frictional elements along its center line. These elements, or beads, are assumed to behave hydrodynamically like spheres whose radius is equal to that of the flagellum; the positions of their centers are determined by the condition of tangential contact between neighboring beads. On the other hand, the body or "head" of the microorganism is represented by a bigger bead whose radius is that of the sphere with the same translational frictional coefficient in the swimming direction as the body.

The bead model is depicted in Fig. 1*a*, where a is the radius of the body, r is the radius of the flagellum, λ is its wavelength, and b is the radius of the helical center line. The helical axis coincides with the x-axis of a laboratory-fixed system of Cartesian coordinates. The x-length of the flagellum is $L_x = n\lambda$, n being the number of wavelengths. The contour length of the flagellum is given by $L_c = n\Lambda$, where Λ is the contour wavelength. This is related to λ through $\Lambda = \lambda/\alpha$, with $\alpha = (1 + k^2b^2)^{-1/2}$ being the cosine of the constant angle between the tangent to the center line and the x-axis. k is the helix wave number, $2\pi/\lambda$. We define δ as the projection on the x-axis of the segment that connects two neighboring beads, as indicated in Fig. 1*b*. The tangency condition leads to the following equation:

$$(\delta/b)^2 + 4\sin^2(kb\delta/2b) - 4(r/b)^2 = 0, \qquad (1)$$

whose solution for δ/b can be obtained by Newton-Raphson iterations. With δ, an alternative expression for the x-length is $L_x = N\delta$.

Each of the N beads on the flagellum moves in the x-direction with the swimming velocity V and rotates simultaneously in the positive θ-direction with angular ve-

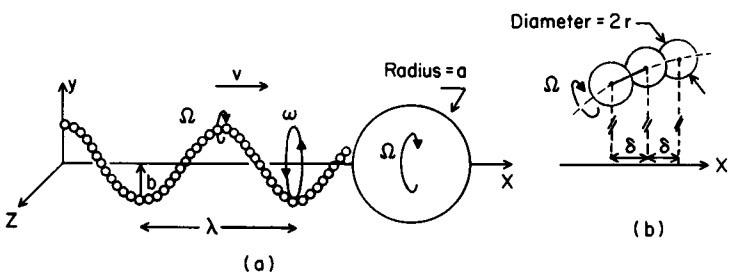

FIGURE 1 (*a*) Bead model for a helical flagellum. Note the three rotations: ω (flagellum), Ω (head), and Ω (flagellum). Symbols are defined in the text. (*b*) Detail of the arrangement of beads. The projections of the beads on the x-axis are equally spaced.

locity ω. Then the position of the ith flagellar bead after time t is given by

$$x_i = \delta i + Vt, \tag{2a}$$

$$y_i = b\cos(kx_i + \omega t) \qquad i = 0, 1, \ldots, N-1, \tag{2b}$$

$$z_i = b\sin(kx_i + \omega t). \tag{2c}$$

The position of the head is given by

$$x_N = L_x + a + Vt, \tag{3a}$$

$$y_N = z_N = 0. \tag{3b}$$

By differentiation of Eqs. 2 and 3, one obtains

$$i = 0, 1, \ldots, N-1 \quad \begin{cases} v_{xi} = V, & (4a) \\ v_{yi} = -b\omega\sin(kx_i + \omega t), & (4b) \\ v_{zi} = b\omega\cos(kx_i + \omega t), & (4c) \end{cases}$$

$$v_{xN} = V, \tag{5a}$$

$$v_{yN} = v_{zN} = 0. \tag{5b}$$

for the Cartesian velocities of the beads. In addition to these velocities, the head must rotate around the x-axis and the flagellum around the tangent of the center line, each with angular velocity Ω in the opposite direction to ω, as indicated in Fig. 1. This fact, discovered by Chwang and Wu (4), is necessary to cancel the total torque, as will be shown later.

Hydrodynamic Interaction

In the preceding section the geometry and kinematics of the helical bead model were presented. Now we will show how the dynamics of the particle can be deduced by using an interaction tensor formalism, as is common in polymer hydrodynamics.

The force exerted on the solvent by the ith bead of the model, $\mathbf{F}_i$, is proportional to the relative velocity $\mathbf{v}_i'$ of the bead with respect to the fluid

$$\mathbf{F}_i = \zeta_i \mathbf{v}_i', \tag{6}$$

where ζ_i is the Stokes' law frictional coefficient of the spherical bead

$$\zeta_i = 6\pi\eta_0 r, \; i = 0, 1, \ldots N-1, \tag{7a}$$

$$\zeta_N = 6\pi\eta_0 a. \tag{7b}$$

η_0 is the viscosity of the fluid, and $\mathbf{v}_i'$ is given by

$$\mathbf{v}_i' = \mathbf{v}_i - \mathbf{u}_i, \tag{8}$$

where $\mathbf{v}_i$ and $\mathbf{u}_i$ are the absolute velocities of bead i (Eqs. 4 or 5) and fluid, respectively, at the position of the bead.

The distribution of point forces acting on the fluid creates a velocity field that superimposes on that which the fluid would have in the absence of the particle. Then, the actual velocity of the fluid at bead i has two components: the unperturbed velocity, $\mathbf{u}_i^0$, and the perturbation arising from the forces from the other beads

$$\mathbf{u}_i = \mathbf{u}_i^0 + \sum_{j=0}^{N}{}' \mathbf{T}_{ij}\mathbf{F}_j. \tag{9}$$

In the case we are studying, the solvent would be at rest if the particle were absent ($\mathbf{u}_i^0 = \mathbf{O}$), so that Eqs. 6, 8, and 9 give us

$$\mathbf{v}_i' = \mathbf{v}_i - \sum_{j=1}^{N}{}' \zeta_j \mathbf{T}_{ij}\mathbf{v}_j' \tag{10}$$

Eq. 10 is the basis of the Oseen-Kirkwood (14,15) theory of hydrodynamic interaction. The prime indicates omission of the term in the sum having $j = i$. $\mathbf{T}_{ij}$ is a third-rank tensor that determines the hydrodynamic interaction between beads i and j. Its expression in a general, curvilinear system of coordinates is (15)

$$(T_{ij})_{\alpha\beta} = \frac{1}{8\pi\eta_0 R_{ij}}\left[C_1 \frac{\partial \mathbf{R}_i}{\partial\alpha}\cdot\frac{\partial \mathbf{R}_j}{\partial\beta} + C_2\frac{[\mathbf{R}_{ij}\cdot\partial\mathbf{R}_i/\partial\alpha][\mathbf{R}_{ij}\cdot\partial\mathbf{R}_j/\partial\beta]}{R_{ij}^2}\right]. \tag{11}$$

$\mathbf{R}_i$ is the vector joining the origin of coordinates and the center of bead i, and $\mathbf{R}_{ij}$ is the vector between beads i and j. In the original formulation, $C_1 = C_2 = 1$, because the spherical beads were treated as point sources of friction and, therefore, Eq. 11 did not contain the radii of the beads. We have recently proposed a modification that takes into account the finite size of the beads, the result being (20,21):

$$C_1 = 1 + (\sigma_i^2 + \sigma_j^2)/3R_{ij}^2, \tag{12a}$$

$$C_2 = 1 - (\sigma_i^2 + \sigma_j^2)/R_{ij}^2. \tag{12b}$$

where $\sigma_i = r$ for $i = 0, 1, \ldots, N-1$ and $\sigma_N = a$.

In Cartesian coordinates, $\mathbf{T}_{ij}$ takes a simple form:

$$(T_{ij})_{\alpha\beta} = \frac{1}{8\pi\eta_0 R_{ij}}\left[C_1\delta_{\alpha\beta} + C_2\frac{(R_{ij})_\alpha (R_{ij})_\beta}{R_{ij}^2}\right], \quad \alpha,\beta = x,y,z, \tag{13}$$

where $\delta_{\alpha\beta}$ is Kronecker's delta. This tensor is symmetric with respect to $i - j$ and $\alpha - \beta$ permutations.

Because of the helical geometry of the flagellum, cylindrical coordinates are much more suitable to express the interaction tensor between its beads. The cylindrical components of $\mathbf{R}_i$ and $\mathbf{v}_i$ are

$$i = 0, 1, \ldots, N-1 \begin{cases} x_i = \delta i + Vt, \; v_{xi} = V, & (14a) \\ \theta_i = k\delta i + \omega t, \; \omega_i = \omega, & (14b) \\ r_i = b, \; \rho_i = 0. & (14c) \end{cases}$$

The cylindrical components of the interaction tensor can be obtained from the definition, Eq. 11, through tedious but straightforward algebra. They are summarized in Appendix I, where a more restrictive symmetry relationship, $(T_{ij})_{\alpha\beta} = (T_{ji})_{\beta\alpha}$, can be noted. The expressions in Appendix I are completely general. When we particularize to helical structures, using Eq. 14, the intraflagellar hydrodynamic interaction tensors, written as dimensionless quantities, are formulated in Appendix II. For head-flagellum tensors, $\mathbf{T}_{iN}$, we prefer to use Cartesian coordinates; the Cartesian components of $\mathbf{T}_{iN}$ can be very easily derived from Eqs. 12, 1, and 3, and we do not reproduce the results here. Lastly, the basic hydrodynamic interaction Eq. 9 can be rewritten as:

$$v'_{xi} + \sum_{j=0}^{N-1}{}' \zeta_j (T_{ij})_{xx} v'_{xj} + \sum_{j=0}^{N-1}{}' \zeta_j (T_{ij})_{x\theta} b^{-1} \omega'_j b + \sum_{j=0}^{N-1}{}' \zeta_j (T_{ij})_{xr} \rho'_j + \sum_{\alpha=x,y,z} \zeta_N (T_{iN})_{x\alpha} v'_{N\alpha} = V; \; i = 0, 1, \ldots, N-1. \tag{15}$$

$$b\omega'_i + \sum_{j=0}^{N-1}{}' \zeta_j (T_{ij})_{\theta x} b^{-1} v'_{xi} + \sum_{j=0}^{N-1}{}' \zeta_j (T_{ij})_{\theta\theta} b^{-2} b\omega'_j + \sum_{j=0}^{N-1}{}' \zeta_j (T_{ij})_{\theta r} b^{-1} \rho'_j + \sum_{\alpha=x,y,z} \zeta_N [(T_{iN})_{z\alpha} \cos\theta_i - (T_{iN})_{y\alpha} \sin\theta_i] v'_{\alpha N} = \omega b; \; i = 0, 1, \ldots, N-1. \tag{16}$$

$$\rho'_i + \sum_{j=0}^{N-1}{}' \zeta_j (T_{ij})_{rx} v'_{xj} + \sum_{j=0}^{N-1}{}' \zeta_j (T_{ij})_{r\theta} b^{-1} b\omega'_j + \sum_{j=0}^{N-1}{}' \zeta_j (T_{ij})_{rr} \rho'_j + \sum_{\alpha=x,y,z} \zeta_N [(T_{iN})_{z\alpha} \sin\theta_i + (T_{iN})_{y\alpha} \cos\theta_i] v'_{\alpha N} = 0; \; i = 0, 1, \ldots, N-1. \tag{17}$$

$$v'_{\alpha N} + \sum_{i=0}^{N-1} \zeta_i (T_{Ni})_{x\alpha} v'_{xi} + \sum_{i=0}^{N-1} \zeta_i [(T_{Ni})_{\alpha Z} \cos\theta_i - (T_{Ni})_{\alpha y} \sin\theta_i] \omega'_i b + \sum_{i=0}^{N-1} \zeta_i [(T_{Ni})_{\alpha y} \cos\theta_i + (T_{Ni})_{\alpha Z} \sin\theta_i] \rho'_i = \delta_{\alpha x} V; \; \alpha = x, y, z. \tag{18}$$

In Eq. 18 $\delta_{\alpha x} = 1$ if $\alpha = x$, and $\delta_{\alpha x} = 0$ when $\alpha \neq x$. Eqs. 15–18 represent a linear system of $3N + 3$ equations. The unknowns are the cylindrical components of the relative velocities of the flagellar beads and the Cartesian components of the head velocity. If this system is solved, Eq. 6 gives a complete description of the forces at each point (bead) of the particle, from which the variables describing the motion can be obtained. In the next two sections methods are proposed to handle the set of linear equations in both exact and approximate ways.

Propulsive and Resistive Forces. Equilibrium Condition.

Eqs. 15–18 can be written in a more compact form.

$$\mathbf{Q}(v'_{x0}, \ldots, v'_{xN-1}, b\omega'_{0}, \ldots, b\omega'_{N-1}, \rho'_{0}, \ldots, \rho'_{N-1}, v'_{xN}, v'_{yN}, v'_{zN})^T = (V, \ldots, V, \omega b, \ldots, \omega b, 0, \ldots, 0, v, 0, 0)^T, \quad (19)$$

where the superscript T indicates a transposed (column) vector and Q is a $(3N + 3)$-rank matrix of coefficients. Let us now define propulsive and repulsive components of forces and velocities. Propulsive components are those that would correspond to a hypothetical case in which the particle were undergoing rotational motion around the x-axis without translating, and can be obtained as the solutions of Eq. 19 when $V = 0$. On the other hand, the resistive components are the solutions of Eq. 19 for $\omega = 0$, and represent the relative velocities associated with a pure translation of velocity V.

The total relative velocities are the sum of the two components:

$$(v'_{x0}, \ldots, v'_{zN})^T = (v'_{x0}, \ldots, v'_{xN})^T_{\text{prop}} + (v'_{x0}, \ldots, v'_{zN})^T_{\text{res}}. \quad (20)$$

Now we take advantage of a property of linear systems: If $\mathbf{x}$ is the solution of $\mathbf{A}\,\mathbf{x} = \mathbf{y}$ and $\mathbf{y} = \mathbf{y}_1 + \mathbf{y}_2$, then $\mathbf{x} = \mathbf{x}_1 + \mathbf{x}_2$ where $\mathbf{x}_1$ and $\mathbf{x}_2$ are the solutions of $\mathbf{A}\mathbf{x}_1 = \mathbf{y}_1$ and $\mathbf{A}\mathbf{x}_2 = \mathbf{y}_2$. If we recall that the resistive and propulsive components correspond to complementary values of the vector in the second hand of Eq. 19, the system can be split and solved as:

$$(v'_{x0}/V, \ldots, v'_{xN-1}/V, b\omega'_0/V, \ldots, b\omega'_{N-1}/V, \rho'_0/V, \ldots, \rho'_{N-1}/V)^T_{\text{res}} = \mathbf{Q}^{-1}(1, \ldots, 1, 0, \ldots, 0, 0, \ldots, 0, 1, 0, 0)^T. \quad (21)$$

$$(v'_{x0}/\omega b, \ldots, v'_{xN}/\omega b, \omega'_0/\omega, \ldots, \omega'_{N-1}/\omega, \rho'_0/\omega b, \ldots, \rho'_{N-1}/\omega b)^T_{\text{prop}} = \mathbf{Q}^{-1}(0, \ldots, 0, 1, \ldots, 1, 0, \ldots, 0, 0, 0, 0)^T. \quad (22)$$

In Eqs. 21 and 22 the velocities have been normalized with V or ωb to yield dimensionless variables. By using Eqs. 6 and 7, expressions can be obtained for the propulsive and resistive forces at each bead, and, by summation over the N beads we can get the components of the total force. For instance, we obtain

$$F_{x(\text{res})}/6\pi\eta_0 aV = v'_{xN(\text{res})}/V + (r/a)\sum_{i=0}^{N-1} v'_{xi(\text{res})}/V, \quad (23a)$$

and

$$F_{x(\text{prop})}/6\pi\eta_0 n\lambda\omega b = (r/n\lambda)\sum_{i=0}^{N-1} v'_{xi(\text{prop})}/\omega b + (a/n\lambda)\, v'_{xN(\text{prop})}/\omega b, \quad (23b)$$

for the resistive and propulsive linear forces in the x-direction.

The most important result of studies on flagellar hydrodynamics is the ratio of

swimming to rotation velocities, $V/\omega b$. It can be obtained by imposing the equilibrium condition for the x-forces, namely, $F_x = F_{(\text{res})} + F_{(\text{prop})} = 0$.
From Eqs. 23,

$$V/\omega b = -\frac{(a/r)v'_{xN(\text{prop})}/\omega b + \sum_{i=0}^{N-1} v'_{xi(\text{prop})}/\omega b}{(a/r)v'_{xN(\text{res})}/V + \sum_{i=0}^{N-1} v'_{xi(\text{res})}/V}. \tag{24}$$

From the solutions of Eqs. 21 and 22, the total relative velocities can be obtained, also as dimensionless forms, in terms of $V/\omega b$:

$$v'_{xi}/V = v'_{xi(\text{res})}/V + (\omega b/V)v'_{xi(\text{prop})}/\omega b, \tag{25a}$$

$$\omega'_i/\omega = (b\omega'_{i(\text{res})}/V)(V/\omega b) + \omega'_{i(\text{prop})}/\omega \quad i = 0, 1, \ldots, N-1, \tag{25b}$$

$$\rho'_i/\omega b = (\rho'_{i(\text{res})}/V)(V/\omega b) + \rho'_{i(\text{prop})}/\omega b, \tag{25c}$$

$$v'_{\alpha N}/V = v'_{\alpha N(\text{res})}/V + (\omega b/V)v'_{\alpha N(\text{prop})}/\omega b \quad \alpha = x, y, z. \tag{25d}$$

The total torque due to ω-rotation of the flagellum, M_{fla}, can be written as

$$M_{\text{fla}}/6\pi\eta_0 n\lambda b^2\omega = (r/n\lambda)\sum_{i=0}^{N-1} \omega'_i/\omega, \tag{26}$$

where $\omega'_i/\omega = (V/\omega b)(b\omega'_{i(\text{res})}/V) + \omega'_{i(\text{prop})}/\omega$. As pointed out previously, to balance this torque, the head and flagellar beads have to rotate around the x-axis and the tangent to the center line. The torques associated with these rotations are $-8\pi\eta_0 \cdot a^3\Omega$ and $-8\pi\eta_0 N r^3 \Omega\alpha$, which, when summed together with M_{fla}, must give zero for the total torque exerted by the particle on the fluid. This second equilibrium condition, corresponding to conservation of angular momentum, leads to

$$\Omega/\omega = \frac{\frac{3}{4}(b^2/r^2)\sum_{i=0}^{N-1} \omega'_i/\omega}{(a/r)^3 + N\alpha}. \tag{27}$$

There are also forces in the radial direction, which come from ρ'_i, v'_{yN} and v'_{zN}. For instance

$$F_y = 6\pi\eta_0 a v'_{yN} + \sum_{i=0}^{N-1} \rho'_i \cos\theta_i, \tag{28}$$

and a similar expression, with $\sin\theta_i$ instead of $\cos\theta_i$, holds for F_z. The modulus and direction of the total radial force are

$$F_r = (F_y^2 + F_z^2)^{1/2}, \tag{29a}$$

$$\theta_r = \tan^{-1}(F_z/F_y). \tag{29b}$$

Lastly, another important characteristic is the hydrodynamic efficiency of the particle. According to Lighthill (10), the efficiency can be related to the energy E dissipated by the ω-rotation per unit of flagellar contour length

$$E = L_c^{-1} 6\pi\eta_0 r\omega b^2 \sum_{i=0}^{N-1} \omega_i'. \tag{30}$$

This energy dissipation does not give any propulsive effect. It is the work required to keep the flagellum rotating to induce the swimming velocity V. Therefore, a measure of the hydrodynamic efficiency is the ratio E/V^2, that can be conveniently formulated as

$$\frac{E}{6\pi\eta_0 V^2} = \frac{r\alpha}{n\lambda}\left(\frac{V}{\omega b}\right)^{-2} \sum_{i=0}^{N-1} \frac{\omega_i'}{\omega} \tag{31}$$

An Approximate Method

The results from the theory developed in the previous sections will be presented and discussed in Results and Discussion. We can anticipate here that the radial components of the velocities of the flagellar beads, ρ_i', take value close to zero over most of the flagellum. Indeed, the angular velocities ω_i' are nearly constant along the flagellum if the sharp variations at the ends are neglected. This suggests an approximate method of calculation in which

$$\omega_i' \equiv \omega' \text{ (constant)}, \rho_i' = 0, i = 0, 1, \ldots, N-1. \tag{32}$$

In Eq. 16, we make the further approximation of averaging the coefficients of v_{xj}' over $i = 0, 1, \ldots, N-1$. Thus, the system of $3N + 3$ equations, 15–18, is transformed into a smaller system with only $N + 4$ equations:

$$v_{xi}' + \sum_{j=0}^{N-1}{}' \zeta_j (T_{ij})_{xx} v_{xj}' + b\omega' \sum_{j=0}^{N-1}{}' \zeta_j (T_{ij})_{x\theta} b^{-1} + \sum_{\alpha=x,y,z} \zeta_N (T_{iN})_{x\alpha} v_{N\alpha}' = V$$
$$i = 0, 1, \ldots N-1. \tag{33}$$

$$b\omega'\left(1 + \frac{1}{N}\sum_{i=0}^{N-1}\sum_{j=0}^{N-1} \zeta_j (T_{ij})_{\theta\theta} b^{-2}\right) + \sum_{j=0}^{N-1} \frac{1}{N}\sum_{i=0}^{N-1} \zeta_j (T_{ij})_{\theta x} b^{-1} v_{xj}'$$
$$+ \sum_{\alpha=x,y,z}\left[\frac{1}{N}\sum_{i=0}^{N-1} (\zeta_N (T_{iN})_{z\alpha} \cos\theta_i - (T_{iN})_{y\alpha} \sin\theta_i)\right] v_{\alpha N}' = bw \tag{34}$$

$$v_{\alpha N}' + \sum_{j=0}^{N-1} \zeta_j (T_{Nj})_{x\alpha} v_{xj}' + \omega' b\left[\sum_{j=0}^{N-1} [(T_{Nj})_{\alpha z} \cos\theta_j - (T_{Nj})_{\alpha y} \sin\theta_i]\right]$$
$$= \delta_{\alpha x} V; \alpha = x, y, z. \tag{35}$$

From the solutions of this smaller system we can compute the approximate values corresponding to the magnitudes defined in Eqs. 23–31. Additional support for this

approximate method, and a comparison of its results with those from the exact treatment, are presented below.

Other Theories

Gray and Hancock (1,2) proposed a theory for swimming of flagellated microorganisms at low Reynolds number conditions expressed in terms of the normal and tangential frictional coefficients of a curvilinear cylinder possessing a periodic shape of small amplitude. These coefficients, per unit of contour length, are

$$C_T = 2\pi\eta_0/\left[\ln(2\lambda/r) - \tfrac{1}{2}\right], \tag{36}$$

and

$$C_N = 2\,C_T. \tag{37}$$

Holwill and Burge (3) were the first who made a complete analysis of the propulsion by helical flagella. Using Gray and Hancock's C_N and C_T, they formulated the equilibrium condition for the force and obtained an expression for $V/\omega b$. Eqs. C.1–C.5 in Appendix C are generalizations, for arbitrary values of C_N and C_T, of some expressions explicitly or implicitely formulated by Holwill and Burge. Later, Chwang and Wu (4) discovered the necessity of a rotation of the head in order to cancel M_{fla}, as explained previously. Chwang and Wu's equations were used to obtain, after minor changes in notation, Eq. C.5 in Appendix C for Ω/ω.

Lighthill (10) has very recently proposed a more rigorous theory, in which the Navier-Stokes equation is solved for the field velocity produced by helical flagella. With small changes in notation and presentation, we have rewritten the most significant of Lighthill's equations in Appendix D. $A_1(\alpha)$, $A_2(\alpha)$, and $A_3(\alpha)$ are integral functions given in graphical form in Figs. 11 and 15 of ref. 10. We have digitized the curves in those figures and fit them to third-degree polynomials in α^2, Eqs. D11–D13, which produce Lighthill's values with deviations smaller than ± 0.01. Although Lighthill's main results are not formulated in terms of frictional coefficients, he gives, as a secondary result from his theory, values for C_T and C_N more accurate than Gray and Hancock's:

$$C_T = 2\omega\eta_0/\ln(0.18\lambda/\alpha r), \tag{38}$$

$$C_N = 4\pi\eta_0/\left[\ln(0.18\lambda/\alpha r) + \tfrac{1}{2}\right]. \tag{39}$$

In the next section we will present results from the theories that we have reviewed here for comparison with our own. The following abbreviations will be used: HBCWGH for Holwill-Burge-Gray-Hancock equations (Appendix C) with Gray-Hancock coefficients, Eqs. 36,37; HBCWLI, the same as above but using Lighthill Eqs. 38,39; LI, Lighthill theory (Appendix D).

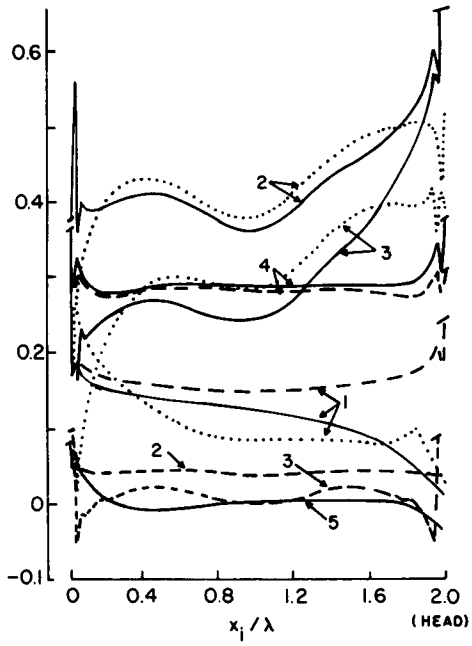

FIGURE 2 Profile of bead velocities along the flagellum, corresponding to a particle with kb = 1.0, r/λ = 0.0141, n = 2.0, and a/λ = 0.25 or a/λ = 0. (————) a/λ = 0.25, exact method; (----) a/λ = 0, exact method; (-------) a/λ = 0.25, approximate method. The abscissa is the reduced x-coordinate of the ith bead, and the head is attached to the right end. Values of the ordinate are as follows: Curve 1, $v'_{xi(\text{res})}/V$; 2, $-v'_{xi(\text{prop})}/V$; 3, $-v'_{xi}/V$; 4, ω'_i/ω; 5, $\rho'_i/\omega b$.

RESULTS AND DISCUSSION

We first present a complete calculation of the quantities characterizing the motion of a hypothetical microorganism that has dimensions within the range of experimental values: kb = 1.0, r/λ = 0.0141, a/λ = 0.25, and n = 2. The flagellum is modeled by 100 beads. The two systems of linear equations, 21 and 22, were solved on a CDC CYBER 74 computer (Control Data Corp., Minneapolis, Minn.) by Gauss-Seidel iterations. In Eqs. 1, 3, and 14 we set ωt = 0. The dependence of the results on t will be discussed later. The solutions of these equations, the propulsive and resistive components of the relative velocities, have been plotted in Fig. 2 as velocity profiles along the x-axis of the flagellum. $\omega'_{(\text{res})}/\omega$ and $\rho'_{(\text{res})}/\omega b$ are nearly zero over the whole flagellum, so that only the total values, ω'_i/ω and $\rho'_i/\omega b$, are plotted in Fig. 2.

Our calculation is the first that gives a quantitative image to the end-effects: they appear as sharp peaks at the tip and base of the flagellum. There are two kinds of end-effects. The first arises from the fact that the number of neighboring beads to the left is different from the number to the right, for beads placed near the ends. This causes strong variations in the velocity profile at the three or four beads at either end

but is insignificant along most of the central part of the flagellum. The second kind of end-effect occurs only at the end connected to the head. It reflects a strong hydrodynamic interaction between the forward motion of the head, which drags a large portion of fluid with it, and the translational-rotational motion of the nearby beads. To illustrate the difference between the two kinds of effects, we have also calculated the relative velocities for a particle without a head. These are represented as dashed lines in Fig. 2. By comparison of the velocity profiles for the two cases ($a/\lambda = 0.25$ and $a/\lambda = 0$), we reach the following conclusions: (*a*) When $a = 0$ there is no end-effect of the second kind. The curves are rather flat (constant) over most of the flagellum and symmetric with respect to its middle. (*b*) For $\alpha \neq 0$, the profile of ω_i'/ω is very close, both in shape and absolute value, to that for $a = 0$, and is practically constant over the whole flagellum. Furthermore, $\rho_i'/\omega b$ is nearly zero. In other words, there are no end-effects of the second kind for ω_i' and ρ_i', irrespective of the value of a. These findings give strong support to the approximate method used earlier. (*c*) The end-effect of the second kind produces a strong variation in $v'_{xi(\text{res})}$ and $v'_{xi(\text{prop})}$ at the side of the flagellum near the head. Holwill and Burge (3), Chwang and Wu (4), and Lighthill (10) neglected end-effects of the first kind, and our results confirm that this is quite reasonable because they affect only a very small part of the flagellum. However, Holwill and Burge and Chwang and Wu also neglected end effects of the second kind, while Lighthill took some account of head-tail hydrodynamic interaction. For this reason, as we will show later, Lighthill's theory gives results much closer to ours than do the other theories.

Results from the approximate method are also included in Fig. 2 (dotted lines). Agreement between the exact method and the approximate one is fair, and discrepancies of different sign at different parts of the flagellum and at the head compensate to give very similar values for $V/\omega b$, Ω/ω, M_{fla}, and E. This is shown in Table I, where the values obtained from each theory for the quantities characterizing the mo-

TABLE I

SWIMMING CHARACTERISTICS OF A MICROORGANISM WITH $kb = 1.0$, $r/\lambda = 0.0141$, $a/\lambda = 0.25$, AND $n = 2$, ACCORDING TO SEVERAL THEORIES

	This work		Other theories		
	Exact method	Approximate method	HBCWGH	HBCWLI	LI
$F_{\text{res}}/6\pi\eta_0 aV$	1.465	1.433	2.270	2.763	—
$F_{\text{prop}}/6\pi\eta_0 n\lambda\omega b$	−0.021	−0.021	−0.053	−0.057	—
$V/\omega b$	0.114	0.118	0.187	0.166	0.136
$F_r/6\pi\eta_0 aV$	0.58	0.57	—	—	—
θ_r(deg.)	37	12	—	—	—
$M_{\text{fla}}/6\pi\eta_0 n\lambda\omega b^2$	0.211	0.205	0.149	0.211	0.214
Ω/ω	0.506	0.493	0.359	0.509	0.519
$\omega/(\omega + \Omega)$	0.664	0.669	0.736	0.663	0.658
$E/6\pi\eta_0 V^2$	11.4	10.4	3.43	5.87	8.20
v'_{xN}/V	1.72	1.67	—	—	—

tion of the particle are presented. Values from our exact and approximate methods are in excellent agreement. We thus conclude that the approximations that we have introduced are physically reasonable and that the approximate method, which requires considerably less computer memory and time, can be used for further calculations without loss of accuracy. Comparison between our theory and the others shows that Lighthill's gives similar results; while the treatments by Holwill and Burge and by Chwang and Wu, based on the frictional coefficients C_T and C_N, lead to quite different values, especially if the Gray and Hancock equations (Eqs. 36,37) are used.

All the results reported in Table I are time-independent, except θ_r. If ωt in Eqs. 1, 3, and 14 is varied, θ_r changes as $\theta_r = 37° + \omega t$. Then, the radial force, F_r, has a constant modulus and oscillates with angular velocity ω. This implies that the center of mass of the particle not only translates but also rotates around the x-axis. The path of the center of mass will be a helix rather than the x-axis, and the radius of the helix will be small, since F_r must take relatively low values. This result was previously obtained by Keller and Rubinow (7).

The effect of a change in head size relative to the flagellum is shown in Fig. 3. $\omega/\cdot(\omega + \Omega)$ represents the ratio of the angular velocity of the flagellum, ω, to that actually generated by the rotatory motor, $\omega + \Omega$. Values of $\omega/(\omega + \Omega)$ from HBCWLI, LI, and our theory (approximate method) coincides over the entire range of a/λ, while HBCWGH deviates in the region of low a/λ (<0.4), where most of the experimentally observed values are expected to fall. LI values for $V/\omega b$ are closer to ours than to the others for small a/λ; while for higher ratios, LI values are intermediate between ours and the others. The reason for this behavior is that head-flagellum interactions are taken into account rigorously in our theory and approximately in LI, but are neglected in HBCWGH and HBCWLI.

Fig. 4 illustrates the effect of varying r/λ on $\omega/(\omega + \Omega)$ and on $V/\omega b$. Calculations with our theory cannot be extended to the 10^{-3} range of r/λ because of the large number of beads needed to model the flagellum. The same trend as in Fig. 3 is observed; results from the Lighthill theory are closer to ours than to those from the other theories over most of the range of r/λ. A singularity is observed for HBCWLI and LI values at $r/\lambda = 0.1$–0.2. This corresponds to $C_T \to \infty$ (Eq. 38) and $\ln\epsilon \to 0$ (Eq. D.8). Fortunately, the observed values of r/λ will be in most cases on the order of 10^{-2}.

To obtain the optimum performance, a microorganism can change the conformation of its flagellum (λ, b) to get the maximum velocity V with a minimum rate of working, E. Lighthill (9,10) has predicted that the optimum performance is obtained when the tangent to the center line makes an angle of 45° ($kb \simeq 1$) with the x-axis, in excellent agreement with experimental data for *Euglena viridis* (22). To study this situation, the configuration of the flagellum corresponding to the microorganism in Table I can be modified without alterating its absolute dimensions (a, r, L_c). This microorganism has $L_c/r = 200$ and $a/r = 17.7$. If we also conserve $n = 2.0$, the value of kb determines completely the geometry of the helix. Fig. 5 shows the dependence on kb of three motional quantities. All the theories predict optimum performance at

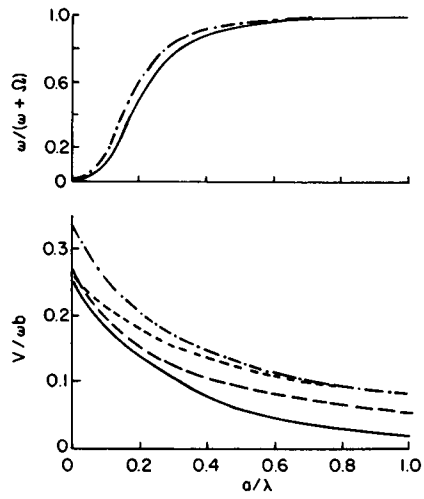

FIGURE 3

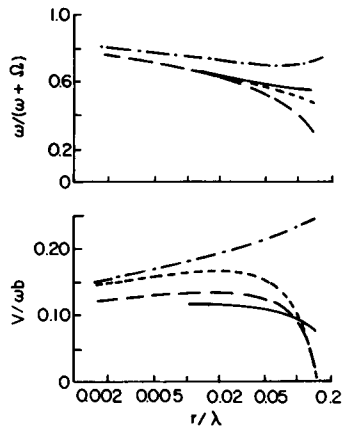

FIGURE 4

FIGURE 3 Variation of $V/\omega b$ and $\omega/(\omega + \Omega)$ with a/λ. The other parameters are the same as in Fig. 2 and Table I: $kb = 1.0$, $r/\lambda = 0.0141$, $n = 2.0$. Key for Figs. 3, 4, and 5: (—·—·—) HBCWGH; (-------), HBCWLI; (———) LI; (————) our theory (bead model, approximate method). Curves for $\omega/(\omega + \Omega)$ from HBCWLI, LI, and our theory are practically coincident.
FIGURE 4 Variation of $V/\omega b$ and $\omega/(\omega + \Omega)$ with r/λ for $kb = 1.0, a/\lambda = 0.25, n = 2$. The symbols for the curves have the same meaning as in Fig. 3.

$kb \simeq 1$, and the extreme position is rather insensitive to variations in the other geometrical parameters. However, the absolute values obtained from the different theories are quite disparate.

Fig. 5 also contains information on viscosity dependence of the swimming velocity. The dimensions a, r, and L_c, and the power output E are fixed for a given particle. On the other hand, the only configurations (or values of b and k) allowed for the flagellum must be those that give the optimum value $kb \simeq 1$, corresponding to the minimum of $E/6\pi\eta_0 V^2$ and maximum of $v/\omega b$. This is so regardless of the value of the viscosity, η_0. Then, if η_0 varies, V should change in such a way that $E/6\pi\eta_0 V^2$ is kept constant at its minimum. Since E is fixed, a relationship $V = \text{const} \cdot \eta_0^{-1/2}$ is obtained. For example, if η_0 changes to $\eta_0' = 4\eta_0$, $V' = \frac{1}{2}V$; to maintain $V/\omega b$ constant at its maximum, $b' = \frac{1}{2}b$, and $k' = 2k$ for constant kb.

Keller (23) used cruder equations by Taylor (24) and Hancock (1) to explain the viscosity dependence of V. He made different assumptions regarding the variations of the flagellar configuration, and did not consider the existence of a maximum in the hydrodynamic efficiency. His calculation predicted $V = \beta_1/(\beta_0 + \eta_0)$, β_0 and β_1 being constants. Available data for *Pseudomonas aeruginosa,* obtained by Schneider and Doetsch (25), are plotted in Fig. 6 as a function of $\eta_0^{-1/2}$. The continuous straight line, $V = 95\eta_0^{-1/2}$, is the best least squares fit to the data according to our considerations, while the discontinuous line is $V = 321./(\eta_0 + 2.61)$, as reported by Keller. Because of the scatter of the data, it cannot be decided which theory gives the best fit.

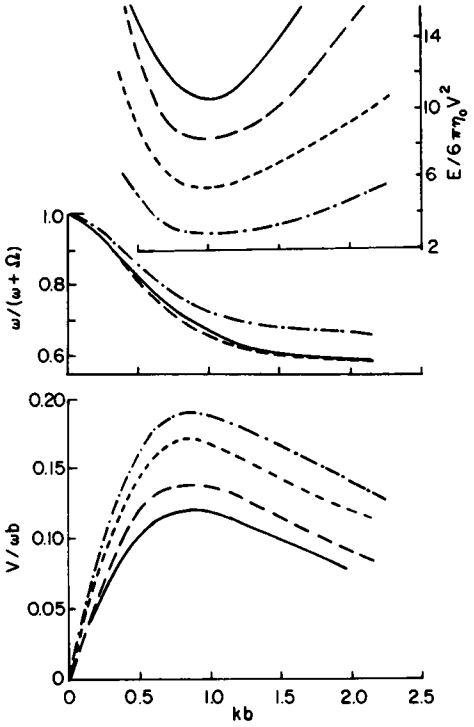

FIGURE 5

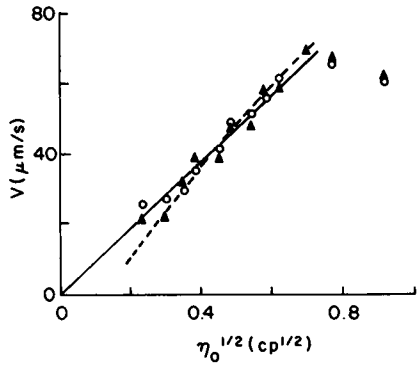

FIGURE 6

FIGURE 5 Variation of $V/\omega b$, $\omega/(\omega + \Omega)$, and $E/6\pi\eta_0 V^2$ with kb for a particle with fixed a, L_c, r, and n. Values $L_c/r = 200$, $a/r = 17.7$, and $n = 2$ have been choosen to match those used in Table I and Figs. 3 and 4. HBCWLI and LI curves for $\omega/\omega + \Omega$) are coincident. See Fig. 3 for the key to the curves.

FIGURE 6 Effect of the viscosity on the swimming velocity. Points are experimental values for *P. aeruginosa* from Schneider and Doetsch (25). Continuous straight line, $V = 95\ \eta_0^{-1/2}$ according to our analysis. Discontinuous line, $V = 321/(\eta_0 + 2.6)$, according to Keller (23).

Our formula has the advantage of requiring only one adjustable constant. Both Keller's analysis and ours fail to explain the decrease in V at low η_0.

It should be remarked that the above analyses of the maximum efficiency and the viscosity dependence of swimming velocities have been based on semi-quantitative characteristics common to all the theories we have been considering.

Several conclusions on the reliability and applicability of the different theories may be drawn from the results we have presented. For instance, those formalisms based on normal and tangential frictional coefficients per unit length (C_N and C_T) (3,4) may be somewhat inaccurate if the Gray-Hancock Eqs. 36 and 37 are used. Lighthill's expressions (10) for C_N and C_T, Eqs. 38 and 39, are more accurate and better grounded physically. Theories in which hydrodynamic interaction is more rigorously taken into account, such as Lighthill's general formulation and our own, are preferable for quantitative purposes, particularly when strong hydrodynamic interaction between the head and the flagellum is expected. Numerical differences between Lighthill's theory and

ours are small, so that the lack of accurate data makes a close comparison with experiment impossible.

In this paper we have studied helical flagella because they offer the simplest geometry. In this case Lighthill's theory has a great advantage: it gives analytical expressions of very easy computability, while our theory requires lengthy digital computations. A next step would be to study sinusoidal flagella, for which the curvature is not constant, so that we can expect that Lighthill's theory will give much more complicated or nonanalytical expressions, while the extension of our theory to this case is straightforward. Both helical and sinusoidal models for flagella and spherical representations of the head are strong idealizations of the shapes actually found in nature. For example, *E. viridis* has a rather elongated, ellipsoidal, or cylindrical head, and its flagellum is attached to the anterior extreme of the head (22). In other microroganisms, the flagellum shows a varying amplitude, wavelength, or cross-section (or several of them) along its axis (26). For these complex geometries the utility of our theory is greatly enhanced. The bead model offers substantial versatility to model the overall shape of the head and flagellum, with beads of equal or different diameters. Once the particle has been suitably modeled, and those expressions have been modified which pertain specifically to a helical geometry, the general formalism we have presented here allows for calculations on microorganisms of any complex shape.

This research was supported in part by National Science Foundation grant PCM 75-22728. J. G. T. is supported by a postdoctoral fellowship from the Committee of Cultural Exchange between the U.S.A. and Spain.

Received for publication 18 April 1977.

REFERENCES

1. HANCOCK, G. J. 1953. The self-propulsion of microscopic organisms through liquids. *Proc. R. Soc. Lond. A. Math. Phys. Sci.* **217**:96.
2. GRAY, J., and G. J. HANCOCK. 1955. The propulsion of sea-urchin spermatozoa. *J. Exp. Biol.* **32**:802.
3. HOLWILL, M. E. J., and R. E. BURGE. 1963. A hydrodynamic study of the motility of flagellated bacteria. *Arch. Biochem. Biophys.* **101**:249.
4. CHWANG, A. T., and T. Y. WU. 1971. A note on the helical movement of microorganisms. *Proc. R. Soc. Lond. B. Biol. Sci.* **178**:327.
5. CHWANG, A. T., T. Y. WU, and H. WINET. 1972. Locomotion of *Spirilla*. *Biophys. J.* **12**:1549.
6. SCHNEIDER, K. E. 1971. The helix as propeller of microorganisms. *J. Biomech.* **4**:73.
7. KELLER, J. B., and S. I. RUBINOW. 1976. Swimming of flagellated microorganisms. *Biophys. J.* **16**:151.
8. BLUM, J. J., and J. LUBLINER. 1973. Biophysics of flagellar motility. *Annu. Rev. Biophys. Bioeng.* **2**:181.
9. LIGHTHILL, M. J. 1975. Mathematical biofluiddynamics. Society for Industrial and Applied Mathematics. Philadelphia, Pa. Chapter 3.
10. LIGHTHILL, M. J. 1976. Flagellar hydrodynamics. *SIAM (Soc. Ind. Appl. Math.) Rev.* **18**:161.
11. WU, T. Y. 1966. The mechanics of swimming. In Biomechanics Y. C. Fung, editor. *Proceedings of the Symposium on Biomechanics, American Society of Mechanical Engineers.* 187.
12. COX, R. G. 1970. The motion of long slender bodies in a viscous fluid. 1. General theory. *J. Fluid Mech.* **44**:791.
13. SHACK, W. J., C. S. FRAY, and T. J. LARDNER. 1974. Observation on the hydrodynamics and swimming motions of mammalian spermatozoa. *Bull. Math. Biol.* **36**:555.
14. OSEEN, C. W. 1927. *Hydrodynamik.* Akademische Verlagsgesellscraft. Leipzig. p. 25.

15. KIRKWOOD, J. G., and J. RISEMAN. 1948. The intrinsic viscosities and diffusion constants of flexible macromolecules in solution. *J. Chem. Phys.* **16**:565.
16. RISEMAN, J., and J. G. KIRKWOOD. 1956. The statistical mechanical theory of irreversible processes in solution of macromolecules. *Rheol. Theor. Appl.* **1**:495.
17. YAMAKAWA, H. 1971. Modern Theory of Polymer Solutions. Harper & Row, Publishers, Inc., New York.
18. GARCÍA DE LA TORRE, J., and A. HORTA. 1976. Sedimentation coefficient and x-ray scattering of a double-helical model for deoxyribonucleic acid. *J. Phys. Chem.* **80**:2028.
19. GARCIA DE LA TORRE, J., and V. A. BLOOMFIELD. 1977. Hydrodynamic properties of macromolecular complexes. I. Translation. *Biopolymers.* In press.
20. GARCIA DE LA TORRE, J., and V. A. BLOOMFIELD. 1977. Hydrodynamic properties of macromolecular complexes. II. Rotation. *Biopolymers.* In press.
21. GARCIA DE LA TORRE, J., and V. A. BLOOMFIELD. 1977. Hydrodynamic properties of macromolecular complexes. III. Bacterial viruses. *Biopolymers.* In press.
22. HOLWILL, M. E. J. 1966. The motion of *Euglena viridis*. The role of flagella. *J. Exp. Biol.* **44**:579.
23. KELLER, J. B. 1974. Effect of viscosity on swimming velocity of bacteria. *Proc. Natl. Acad. Sci. U.S.A.* **71**:3253.
24. TAYLOR, G. I. 1951. The action of waving cylindrical tails in propelling microscopic organisms. *Proc. R. Soc. Lond. A. Math. Phys. Sci.* **209**:447.
25. SCHNEIDER, W. R., and R. N. DOETSCH. 1974. Effect of viscosity on bacterial motility. *J. Bacteriol.* **117**:696.
26. HOLWILL, M. E. J., and R. COAKLEY. 1972. Propulsion of microorganisms by three-dimensional flagellar waves. *J. Theor. Biol.* **35**:525.

APPENDIX A

COMPONENTS OF THE INTERACTION TENSOR IN CYLINDRICAL COORDINATES

α	β	$(8\pi\eta_0 R_{ij})^{-1}(T_{ij})_{\alpha\beta}$
x	x	$C_1 + C_2 R_{ij}^{-2}(x_j - x_i)^2$
x	θ	$C_2 R_{ij}^{-2}(x_j - x_i) r_i r_j \sin(\theta_j - \theta_i)$
x	r	$C_2 R_{ij}^{-2}(x_j - x_i)[r_j - r_i \cos(\theta_j - \theta_i)]$
θ	x	$C_2 R_{ij}^{-2}(x_j - x_i) r_i r_j \sin(\theta_j - \theta_i)$
θ	θ	$C_1 r_i r_j \cos(\theta_j - \theta_i) + C_2 R_{ij}^{-2} r_i^2 r_j^2 \sin^2(\theta_j - \theta_i)$
θ	r	$C_1 r_i \sin(\theta_j - \theta_i) + C_2 R_{ij}^{-2} r_i r_j \sin(\theta_j - \theta_i)[r_j - r_i \cos(\theta_j - \theta_i)]$
r	x	$C_2 R_{ij}^{-2}(x_j - x_i)[r_j \cos(\theta_j - \theta_i) - r_i]$
r	θ	$-C_1 r_j \sin(\theta_j - \theta_i) + C_2 R_{ij}^{-2} r_i r_j \sin(\theta_j - \theta_i)[r_j \cos(\theta_j - \theta_i) - r_i]$
r	r	$C_1 \cos(\theta_j - \theta_i) + C_2 R_{ij}^{-2}[r_j - r_i \cos(\theta_j - \theta_i)][r_j \cos(\theta_j - \theta_i) - r_i]$

APPENDIX B

Interaction tensors $(T_{ij})_{\alpha\beta}$, with $\alpha, \beta = x, \theta, r$, for $i, j = 0, 1, \ldots, N-1$

$$\zeta_j(T_{ij})_{xx} = \zeta_i(T_{ji})_{xx} = (3r/4R_{ij})(Q_1 + Q_2\delta^2(j-i)^2/R_{ij}^2), \tag{B.1}$$

$$\zeta_j(T_{ij})_{x\theta}b^{-1} = \zeta_i(T_{ji})_{\theta x}b^{-1} = (3r/4R_{ij})Q_2 b\delta(j-i)\sin(k\delta(j-i))/R_{ij}^2 \tag{B.2}$$

$$\zeta_j(T_{ij})_{xr} = \zeta_j(T_{ji})_{rx} = (3r/4R_{ij})Q_2 b\delta(j-i)[1-\cos(k\delta(j-i))]/R_{ij}^2, \tag{B.3}$$

$$\zeta_j(T_{ij})_{\theta\theta}b^{-2} = \zeta_i(T_{ji})_{\theta\theta}b^{-2}$$
$$= (3r/4R_{ij})[Q_1\cos(k\delta(j-i)) + Q_2b^2\sin^2(k\delta(j-i))/R_{ij}^2], \quad \text{(B.4)}$$

$$\zeta_j(T_{ij})_{\theta r}b^{-1} = \zeta_i(T_{ji})_{r\theta}b^{-1} = (3r/4R_{ij})[Q_1\sin(k\delta(j-i))$$
$$+ Q_2b^2\sin(k\delta(j-i))[1-\cos(k\delta(j-i))]/R_{ij}^2] \quad \text{(B.5)}$$

$$\zeta_j(T_{ij})_{rr} = \zeta_i(T_{ji})_{rr}$$
$$= (3r/4R_{ij})[Q_1\cos(k\delta(j-i)) + Q_2b^2[1-\cos(k\delta(j-i))]^2/R_{ij}^2], \quad \text{(B.6)}$$

$$\zeta_j(T_{ij})_{\theta x}b^{-1} = \zeta_i(T_{ji})_{x\theta}b^{-1} = \zeta_j(T_{ij})_{x\theta}b^{-1}, \quad \text{(B.7)}$$

$$\zeta_j(T_{ij})_{rx} = \zeta_i(T_{ji})_{xr} = -\zeta_j(T_{ij})_{xr}, \quad \text{(B.8)}$$

$$\zeta_j(T_{ij})_{r\theta}b^{-1} = \zeta_i(T_{ji})_{\theta r} = -\zeta_j(T_{ij})_{\theta r} \quad \text{(B.9)}$$

The interbead distances are given by

$$R_{ij} = [\delta^2(j-i)^2 + 4b^2\sin(k\delta(j-i)/2)]^{1/2}. \quad \text{(B.10)}$$

APPENDIX C

Holwill-Burge-Chwang-Wu (3,4) equations are:

$$F_{res}/6\pi\eta_0aV = 1 + n\lambda\alpha(C_Nk^2b^2 + C_T)/6\pi\eta_0a, \quad \text{(C.1)}$$

$$F_{prop}/6\pi\eta_0n\lambda\omega b = kb\alpha(C_N - C_T)/6\pi\eta_0, \quad \text{(C.2)}$$

$$M_{fla}/6\pi\eta_0n\lambda\omega b^2 = (\alpha C_T/6\pi\eta_0)[C_N/C_T + k^2b^2$$
$$- (C_N/C_T - 1)^2k^2b^2/(1 + A + k^2b^2C_N/C_T)], \quad \text{(C.3)}$$

$$V/\omega b = (C_N/C_T - 1)kb/(1 + A + k^2b^2C_N/C_T), \quad \text{(C.4)}$$

$$\Omega/\omega = [(1 + k^2b^2C_N/C_T + A)(C_N/C_T + k^2b^2) - (C_N/C_T - 1)^2k^2b^2]/$$
$$(1 + A + k^2b^2C_N/C_T)B, \quad \text{(C.5)}$$

$$E/6\pi\eta_0V^2 = (\alpha^2C_T/6\pi\eta_0)(1 + A + k^2b^2C_N/C_T)\cdot$$
$$[(C_N/C_T + k^2b^2)(1 + A + k^2b^2C_N/C_T)/k^2b^2(C_N/C_T - 1)^2 - 1], \quad \text{(C.6)}$$

where

$$A = (3\pi\eta_0/C_T)(2a/n\lambda\alpha), \quad \text{(C.7)}$$

$$B = (3\pi\eta_0/C_T)(16\pi^2/3k^2b^2)[(r/\lambda)^2 + (a/\lambda)^3 2/n\alpha]. \quad \text{(C.8)}$$

APPENDIX D

Lighthill (10) equations:

$$V/\omega b = (1 + \psi a\alpha/n\lambda)^{-1}(kb)^{-1}\chi_0(1-\alpha^2)[-1 - \ln\epsilon + A_1(\alpha)], \quad \text{(D.1)}$$

$$\Omega/\omega = (1 + \Psi a\alpha/n\lambda)(1 + \psi a\alpha/n\lambda)^{-1}\chi_0 nk^2b^2/[8\pi^2\alpha(a/\lambda)^3], \quad (D.2)$$

$$M_{\text{fla}}/(6\pi\eta_0 n\lambda\omega b^2) = (1 + \Psi a\alpha/n\lambda)(1 + \psi a\alpha/n\lambda)^{-1}(2\chi_0/3\alpha), \quad (D.3)$$

$$E/(6\pi\eta_0 V^2) = (1 + \Psi a\alpha/n\lambda)(1 + \psi a\alpha/n\lambda)^{\frac{2}{3}}\{\chi_0\alpha^2(1 - \alpha^2) [-1 - \ln\epsilon - A_1(\alpha)]^2\}^{-1}, \quad (D.4)$$

where

$$\chi_0 = [-(1 - \alpha^2) - (2 - \alpha^2)\ln\epsilon + \alpha^2 A_1(\alpha) + 2(1 - \alpha^2)A_2(\alpha)]^{-1}, \quad (D.5)$$

$$\Psi = \tfrac{3}{2}Q^{-1}[2 - \alpha^2 - 3\alpha^{-1} + 2\alpha^{-1}\ln(2\pi n) - (1 + \alpha^2)\ln\epsilon - 2A_3(\alpha) - (1 - \alpha^2)A_1(\alpha)], \quad (D.6)$$

$$\psi = \Psi - \tfrac{3}{2}\chi_0\alpha^2(1 - \alpha^2)[-1 - \ln\epsilon + A_1(\alpha)]^2, \quad (D.7)$$

$$Q = 1 + \frac{\ln(n\lambda/a) - \frac{3}{2}}{2\ln(2\pi n) + 2\ln(2\pi\zeta/\lambda) - 4}, \quad (D.8)$$

$$2\ln(2\pi\zeta/\lambda) = -\alpha + \alpha^3 + \alpha(1 + \alpha^2)\ln\epsilon + 2\alpha A_3(\alpha) + \alpha(1 - \alpha^2)A_1(\alpha) + 1 - \alpha, \quad (D.9)$$

$$\epsilon = \sqrt{e}\pi r\alpha/\lambda = 5.1796\, r\alpha/\lambda \quad (D.10)$$

$$A_1(\alpha) = 0.140 + 1.395\,\alpha^2 - 1.885\,\alpha^4 + 0.774\,\alpha^6, \quad (D.11)$$

$$A_2(\alpha) = 0.694 - 1.247\,\alpha^2 + 1.357\,\alpha^4 - 0.577\,\alpha^6, \quad (D.12)$$

$$A_3(\alpha) = 2.961 - 9.10\,\alpha^2 + 10.22\,\alpha^4 - 4.10\,\alpha^6, \quad (D.13)$$